Spatial Scaling and Variability of Soil Moisture Over Heterogeneous Land Cover and Dynamic Vegetation Conditions

Karthik Nagarajan, *Member, IEEE*, and Jasmeet Judge, *Senior Member, IEEE*

***Abstract*—In this letter, near-surface and root-zone soil moisture (RZSM), land surface temperature (LST), leaf area index, and vegetation water content were simulated at different spatial scales for three land cover types in North Central Florida under dynamic vegetation conditions. Insights into expected retrieval errors in soil moisture (SM) due to assumptions of static landscape were obtained from differences in the estimates using the static and dynamic land covers. Maximum differences of about 0.04 m^3/m^3 in near-surface SM and RZSM, and 5.1 K in LST were observed between estimates obtained over the vegetated and bare-soil regions during dry-soil conditions. During wet conditions, the maximum differences in near-surface SM and RZSM increased to about 0.05 m^3/m^3, while those in LST decreased to 3.6 K. The RZSM simulations generated at the two resolutions of 200 m and 10 km were used to implement an upscaling algorithm based on averaging, to illustrate the use of the synthetic data set for upscaling studies. This letter highlights the importance of simulating land surface states at multiple scales for heterogeneous landscapes under dynamic vegetation conditions and for developing accurate SM retrieval and scaling algorithms.**

***Index Terms*—Downscaling, dynamic vegetation, root-zone soil moisture (RZSM), Soil Moisture Active Passive (SMAP), Soil Moisture and Ocean Salinity (SMOS), upscaling.**

I. Introduction

THE availability of soil moisture (SM) products from the recent Soil Moisture and Ocean Salinity (SMOS) mission and the upcoming Soil Moisture Active Passive (SMAP) mission will provide unprecedented SM information on a global basis for research in hydrology, agricultural productivity, and water-resource management. The SMOS provides SM at a spatial resolution of 45 km every two to three days [1]. The SMAP mission will provide an SM product at 9 km [2] by combining active and passive microwave observations. These products have to be downscaled to field scales of 200 m–1 km for applications in hydrology and agriculture, and to study the impact of subpixel SM variability caused by land surface heterogeneity, climatic variability, and dynamic vegetation within the satellite footprint. Unfortunately, a dense network of field measurements is typically unavailable under the satellite footprint to evaluate the spatial scaling algorithms. An effective alternative is to develop a synthetic experiment for simulating SM observations at both satellite and field scales by embedding various factors that contribute to spatiotemporal dynamics in SM.

Spatial variability in surface SM is driven by complex interactions among soil texture, topography, climate, land cover, and vegetation [3], [4]. Heterogeneity in soil texture and topography impact spatiotemporal distribution of SM by affecting soil water balance processes [5]. Spatiotemporal variability in SM is also driven by micrometeorological factors such as solar radiation, air temperature, wind velocity, relative humidity, and precipitation, with precipitation providing the most impact on SM variability [6]. Spatial fields of SM are also affected by land cover characteristics through the processes of infiltration and evapotranspiration, particularly in agricultural landscapes [7]–[9]. Such landscapes are representative of dynamic vegetation conditions, characterized by crop growth and development cycles. In addition, crop management schedules, such as irrigation, applications of fertilizer, growth regulators, and pesticides, impact crop growth. Existing simulation frameworks, such as the SMAP testbed [10], [11], do not consider crop management. A simulation framework that generates SM fields of heterogeneous landscapes at multiple resolutions over growing seasons of crops is also essential to evaluate spatial scaling algorithms.

The primary goal of this letter is to develop a simulation framework for generating land surface and vegetation states, such as volumetric SM within 0- to 5-cm depth (VSM_{0-5}), root-zone SM (RZSM) within 0- to 1-m depth, land surface temperature (LST), leaf area index (LAI), and vegetation water content (VWC), at multiple scales for heterogeneous land cover, as well as dynamic vegetation and hydrometeorological conditions. The three objectives of this letter are the following: 1) to simulate VSM_{0-5}, RZSM, LST, LAI, and VWC at resolutions of 200 m and 10 km, representative of agricultural fields and a SMAP SM pixel, respectively; 2) to analyze the impact of vegetation and precipitation on spatial fields of VSM_{0-5}, RZSM, and LST; and 3) to demonstrate the significance of simulations available across multiple scales by implementing a simple upscaling algorithm based on averaging. This simulation framework can be also used for other studies that require synthetic observations of land surface states and crop growth under heterogeneous land cover conditions at multiple scales. The simulated observations across multiple scales can be also used to analyze the impact of various error sources on microwave remote sensing products.

Manuscript received September 16, 2011; revised January 31, 2012, March 13, 2012, and May 18, 2012; accepted May 30, 2012. Date of publication January 21, 2013; date of current version February 20, 2013. This work was supported by the National Aeronautics and Space Administration under the Terrestrial Hydrology Program NNX09AK29G.

The authors are with the Center for Remote Sensing, Agricultural and Biological Engineering Department, University of Florida, Gainesville, FL 32611 USA (e-mail: nagkart@ufl.edu).

Digital Object Identifier 10.1109/LGRS.2012.2226430

1545-598X/$31.00 © 2013 IEEE

In the succeeding section, we describe the simulation framework and the coupled soil-vegetation-atmosphere transfer (SVAT) crop growth model used in this letter.

II. Simulation Framework for SM Scaling Studies

A. Introduction to Simulation Framework

A simulation framework was developed to generate synthetic observations of SM in heterogeneous agricultural landscapes with dynamic vegetation. A 50×50 km^2 area, equivalent to a SMOS pixel, was chosen in North Central Florida as the study region. This region includes a 200×200 m^2 field site at the University of Florida/Institute of Food and Agricultural Sciences Plant Science Research and Education Unit (PSREU), Citra, FL, where a series of season-long field experiments, i.e., the Microwave, Water, and Energy balance eXperiments (MicroWEXs), have been conducted for various agricultural land cover types over the last decade [12]–[14]. Spatial resolutions of 200 m and 10 km were chosen for the simulations, corresponding to the MicroWEX field site and a SMAP SM pixel, respectively. Model simulations were generated for two years, from January 1, 2007, through December 31, 2007. About 95% of the region is comprised of sandy soils, with $> 70\%$ sand by volume in the root zone. Topographic features, including slope, were not considered in this letter because the region is typically characterized by flat terrain, with no runoff in such highly sandy soils. The soil properties, such as porosity, pore-size index, saturated hydraulic conductivity, and air-entry pressure, were assumed to be constant over the region. Vegetation dynamics during the growing seasons, crop management, and precipitation are primary factors impacting the intraseason SM spatial structure in the study region [9]. The simulation framework consisted of three components: a component to simulate meteorological forcings and land cover at 200-m resolution; a coupled SVAT-crop growth model component to simulate soil and vegetation states under growing vegetation; and a component to generate observations at resolutions of 200 m and 10 km.

B. Meteorological Forcings and Land Cover

Fifteen-minute observations of precipitation, relative humidity, air temperature, downwelling solar radiation, and wind speed were obtained from eight Florida Automated Weather Network stations [15]. The observations were spatially interpolated using splines to generate the meteorological forcings at resolutions of 200 m and 10 km. Long-wave solar radiation was estimated following Brutsaert [16]. A 50×50 km^2 landscape was synthetically generated at a resolution of 200 m, with three primary agricultural land cover types, i.e., sweet corn, cotton, and bare soil (see Fig. 1). A highly dynamic landscape was considered, with two seasons of sweet corn per year, the first season of which starting in March [day of year (DoY) 61–139] and the second in July (DoY 183–261) at the same location, and one season of cotton planted in June (DoY 153–332). Bare-soil conditions were assumed during other times at these locations. Irrigation and crop management schedules for both crops were based upon typical management practices in the region from the field observations during the MicroWEXs and from the farm managers at the PSREU.

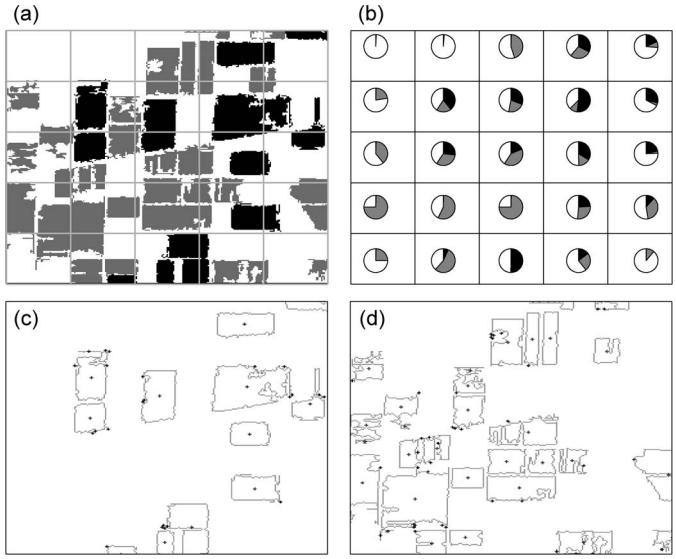

Fig. 1. (a) Land cover at 200 m during cotton and sweet-corn seasons overlaid on a 10-km grid cell. White, gray, and black shades represent bare soil, cotton, and sweet-corn regions, respectively. (b) Pie charts of land cover fractions of (white) bare soil, (gray) sweet corn, and (black) cotton in each 10-km grid. Homogeneous crop fields along with centers for (c) sweet corn and (d) cotton.

C. Coupled SVAT-Crop Growth Model

The SVAT model used in this letter is the land surface process (LSP) model [17]. It simulates 1-D coupled energy and moisture transport in soil and vegetation using diffusion type equations [18], [19] and estimates energy and moisture fluxes at the land surface and in the root zone. The model is forced with micrometeorological parameters such as air temperature, relative humidity, downwelling solar and longwave radiation, irrigation/precipitation, and wind speed. The model has been rigorously tested and extended to wheat stubble [20] and brome grass [21] in the Great Plains, prairie wetlands in Florida [22], tundra in the Arctic [23], and growing crops [24]. The vegetation energy balance is calculated using the model developed in [25] for the water drainage from canopy, the bulk transfer approach for the sensible heat flux from [26], and the latent heat flux following [27]. A block-centered finite-difference scheme is employed to solve the coupled governing equations for water and energy transport in the soil at an adaptive time step in response to the forcings.

The LSP model was coupled to a vegetation growth model, viz., the Decision Support System for Agrotechnology Transfer (DSSAT) to provide the flux estimates during dynamic vegetation conditions [24]. The DSSAT simulates crop growth and development at a daily time resolution using modules for soil, soil–plant–atmosphere, weather, and management, including irrigation and fertilization [28]. The DSSAT model includes modules for over 25 types of crops, including corn, soybeans, wheat, cotton, and different grass types for pasture. The model has been extensively tested in different hydroclimatic regions [28]–[30]. The model was also tested and calibrated for its

applicability to North Central Florida [31] before it was coupled with the LSP model. In the coupled LSP-DSSAT model, the LSP model provides DSSAT with estimates of SM and temperature profiles and evapotranspiration. The DSSAT model provides LSP with vegetation characteristics that influence heat, moisture, and radiation transfer at the land surface and in the vadose zone. The parameters used in the LSP-DSSAT model for both the sweet-corn and cotton models were from [24]. VSM_{0-5} and RZSM are calculated as

$$\theta = \frac{\sum_{i=1}^{m} \mathrm{VSM}_i \Delta z_i}{\sum_{i=1}^{m} \Delta z_i} \tag{1}$$

where θ is SM, m is the total number of nodes (blocks) in either near surface (0–5 cm) or root zone (0–1 m), Δz_i is the thickness of the ith node, and VSM_i is the volumetric SM at the ith node.

D. Observations at Resolutions of 200 m and 10 km

The model simulations were performed over each agricultural field, rather than all the pixels, to reduce computation time. Based upon land cover information at 200 m, contiguous homogeneous regions of sweet corn and cotton were identified, as shown in Fig. 1. A realization of the LSP-DSSAT model was used to simulate VSM_{0-5}, RZSM, LST, LAI, and VWC at the centroid of each homogeneous region, using the corresponding crop module within DSSAT. LST refers to the surface soil temperature during bare-soil conditions and to the canopy temperature in the presence of crops. Zero-mean Gaussian noise, with a standard deviation proportional to that observed in precipitation, was added to the model simulations obtained at the centroid. The ratio of the range of precipitation and the range of each state over the study region was used as the coefficient of proportionality. This accounted for meteorological variability in obtaining spatially distributed VSM_{0-5}, RZSM, LST, LAI, and VWC over each field.

At the 10-km resolution, a realization of the LSP-DSSAT model for each land cover, i.e., sweet corn, cotton, and bare soil, was used to generate three sets of VSM_{0-5} estimates, i.e., θ_{corn}, θ_{cotton}, and $\theta_{\mathrm{baresoil}}$, respectively. The three estimates of VSM_{0-5} obtained over every 10×10 km^2 pixel were combined as a weighted average ($\theta = w_{\mathrm{corn}}\theta_{\mathrm{corn}} + w_{\mathrm{cotton}}\theta_{\mathrm{cotton}} + w_{\mathrm{baresoil}}\theta_{\mathrm{baresoil}}$). Weights w_{corn}, w_{cotton}, and w_{baresoil} represent the fraction of sweet-corn, cotton, and bare-soil pixels at 200 m within each 10×10 km^2 pixel, as shown in Fig. 1(b). Simulated estimates of other states at 10 km were obtained using the same procedure as that for VSM_{0-5}. No errors were added to the simulated estimates generated at 10 km so that the true SM and temperature fields could be analyzed across the two scales. This approach for generating observations at 10 km can be extended to obtain simulations at other resolutions.

III. Results

A. Impact of Heterogeneous Land Cover on SM and LST

Fig. 2 compares 15-min estimates of VSM_{0-5}, RZSM, VWC, and LAI generated over sweet-corn and cotton pixels to those obtained over the same pixel assuming it was unvegetated. Similar estimates of RZSM and VSM_{0-5} are obtained over the sweet-corn [see Fig. 2(a) and (c)] and cotton [see Fig. 2(b) and (d)] pixels in comparison with the bare-soil pixel until planting. However, differences are observed during times of crop growth. As shown in Fig. 2(g) and (h), LAI decreases during the end of growing seasons for both corn (DoY 250–261) and cotton (DoY 250–332), but VWC increases [see Fig. 2(e) and (f)] resulting in significant differences in SM between the vegetated and unvegetated pixels. Differences in the time-averaged estimates of states obtained over vegetated pixels and bare-soil pixels at 200 m were computed from DoY 201–261 to quantify the SM differences over the study region during dynamic vegetation. The differences in VSM_{0-5}, RZSM, and LST were 0.01 $\mathrm{m}^3/\mathrm{m}^3$, 0.011 $\mathrm{m}^3/\mathrm{m}^3$, and 2.4 K, respectively. As shown in Fig. 3, the probability density functions (pdf's) of the three states estimated over all vegetated and bare-soil pixels show the differences in SM and LST. The differences in VSM_{0-5} and RZSM estimated between vegetated and bare-soil pixels increased to 0.015 and 0.016 $\mathrm{m}^3/\mathrm{m}^3$ during days of heavy vegetation (DoY 242–261).

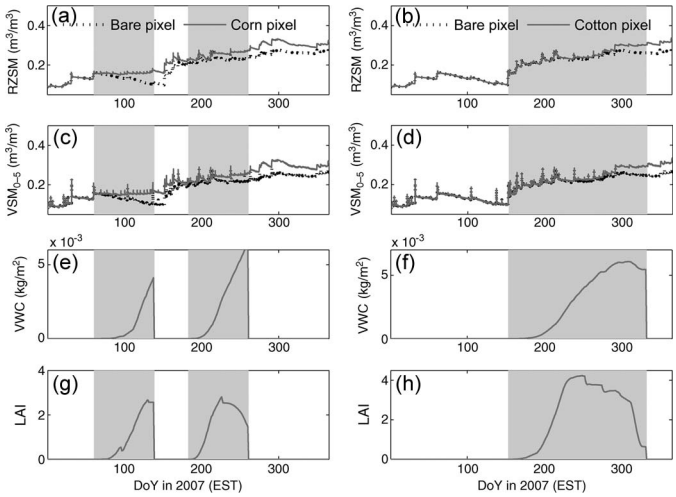

Fig. 2. Simulations of RZSM, VSM_{0-5}, VWC, and LAI for (a), (c), (e), and (g) a sweet-corn pixel and (b), (d), (f), and (h) a cotton pixel in comparison with the same pixel assuming it was unvegetated. Shaded areas depict days of crop growth.

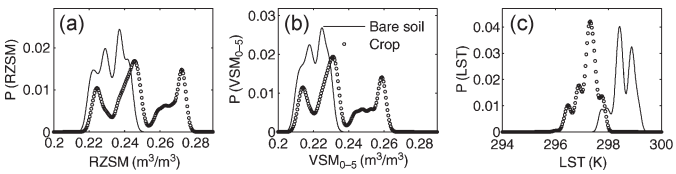

Fig. 3. PDFs of (a) RZSM, (b) VSM_{0-5}, and (c) LST for bare-soil and vegetated pixels estimated from DoY 201–261 over the study region.

B. Impact of Vegetation and Precipitation on Spatial Fields of SM and LST

The simulations on days of dry (DoY 232) and wet (DoY 261) soil conditions were analyzed to study the combined impacts of vegetation and precipitation on spatial fields of SM

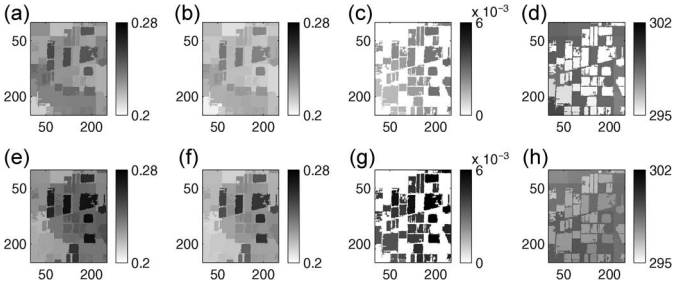

Fig. 4. Simulations of RZSM (in m^3/m^3), VSM_{0-5} (in m^3/m^3), VWC (in kg/m^2), and LST (in kelvins) on DoY (a), (b), (c), and (d) 232 and (e), (f), (g), and (h) 261 at 6 A.M.

TABLE I
DIFFERENCES IN VSM_{0-5} (m^3/m^3), RZSM (m^3/m^3), AND LST (IN KELVINS) COMPUTED BETWEEN SWEET-CORN (S)/COTTON (C) AND BARE-SOIL REGIONS AT 200 M ON DOY 232 AND 261

DoY	Crop	ΔRZSM		ΔVSM_{0-5}		ΔLST	
		Max	Mean	Max	Mean	Max	Mean
232	S	0.030	0.005	0.025	0.005	5.1	3.4
	C	0.045	0.017	0.039	0.015	4.8	3.5
261	S	0.032	0.005	0.026	0.004	3.6	1.5
	C	0.055	0.034	0.052	0.031	3.0	1.1

and LST (see Fig. 4). The differences between the estimates of SM obtained in the bare-soil and vegetated pixels were about 0.032 and 0.038 m^3/m^3 for VSM_{0-5} and RZSM, respectively, during dry conditions [see Table I and Fig. 4(a) and (b)]. These differences increased to about 0.039 and 0.044 m^3/m^3, respectively, after precipitation events due to water retention in vegetated pixels, as shown in Fig. 4(e) and (f).

The pdf's of VSM_{0-5} and RZSM computed over sweet corn, cotton, and bare soil on these two days illustrate the increase in SM variations from bare soil to vegetated conditions, as shown in Fig. 5(a) and (b), (d) and (e). While the differences in SM increased during precipitation, the differences in LST computed between vegetated and bare-soil pixels decreased by 2 K [see Fig. 5(c) and (f), and also Table I]. These estimates of SM and LST, along with surface roughness and vegetation characteristics can be used to estimate remote sensing signatures, such as brightness temperatures and backscattering coefficients, via emission and backscattering models. Products such as SM, LST, and vegetation characteristics, retrieved from the remote sensing observations, can be compared with the simulated estimates to study the impacts of vegetation, resolution, and land cover heterogeneity on various retrieval algorithms. The differences in VSM_{0-5} give an index of retrieval errors that can be expected from SMOS/SMAP when land cover heterogeneity and dynamic vegetation conditions are not considered or are unavailable at the scale of the study.

In spite of resolution degradation expected at 10 km, the range of VSM_{0-5} and RZSM values obtained at 10 km were similar to those obtained at 200 m. The pdf's of VSM_{0-5} and RZSM computed at the two resolutions are centered on mean VSM_{0-5} of about 0.022 m^3/m^3 and mean RZSM of about 0.23 m^3/m^3, but the pdf's at 10 km have a smaller standard deviation, indicating less heterogeneity [see Fig. 6(a) and (b)]. The impact of resolution degradation is larger on LST than

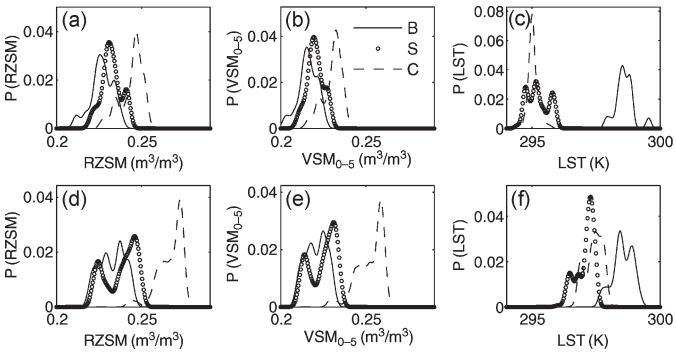

Fig. 5. PDFs of RZSM, VSM_{0-5}, and LST for (B) bare soil, (S) sweet corn, and (C) cotton on DoY (a), (b), and (c) 232 and (d), (e), and (f) 261.

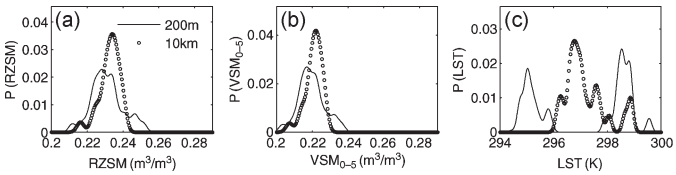

Fig. 6. PDFs of (a) RZSM, (b) VSM_{0-5}, and (c) LST simulated at 200 m and 10 km on DoY 232.

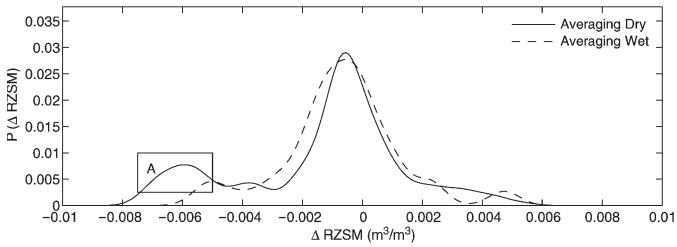

Fig. 7. PDFs of RZSM differences computed between the upscaled estimates and the 10-km simulations during dry- and wet-soil conditions.

that on SM in simulations. Fig. 6(c) shows the degradation of LST heterogeneity at 10-km resolution, where the bimodal distribution of LST observed at 200 m is reduced to a unimodal distribution. Since LST denotes the canopy temperature during crop growth, it shows greater spatial variability, hence the bimodality, than VSM_{0-5} or RZSM at 200 m.

C. Upscaled Estimates of RZSM Using Averaging

The significance of simulating land surface states at multiple scales for dynamic and heterogeneous land cover is demonstrated using a simple upscaling algorithm based on averaging. The framework can be also utilized by more sophisticated scaling algorithms. RZSM generated at 200 m and 10 km during equal lengths of dry (DoY 228-234) and wet (DoY 258-264) soil periods were used for upscaling. Upscaled estimates of RZSM at 10 km were obtained by averaging the estimates at 200 m over every 10×10 km^2 area in the study region. The pdf's of differences between RZSM estimates obtained from the upscaling algorithm and those obtained from the simulation framework are shown in Fig. 7. While the algorithm underestimates RZSM in general, errors on the order of 0.01 m^3/m^3 are observed during dry conditions (see marker A in Fig. 7).

IV. Summary and Conclusion

A novel simulation framework, capable of generating soil and vegetation states on multiple spatial scales, has been developed for a heterogeneous landscape under dynamic vegetation conditions. The simulations enabled the study of combined impacts of vegetation and precipitation on SM and LST. During precipitation events, errors of about 0.052 m^3/m^3 in VSM_{0-5} and about 0.055 m^3/m^3 in RZSM have been observed when vegetation conditions were not considered during SM simulations. These errors are significantly larger than those from the *in situ* sensors, where the standard deviation is typically 0.02 m^3/m^3. Errors of about 5 K can be observed in LST under dynamic vegetation during dry conditions. The aforementioned errors are expected to spatially vary when heterogeneity in soil texture is considered. Loss of heterogeneity has been observed in LST based upon the simulated estimates at 200 m and 10 km, with maximum impacts during dry conditions. The simulations at multiple scales are essential for evaluating scaling algorithms, in terms of their ability to preserve heterogeneity during the scaling process and for developing multiscale models of land surface processes over heterogeneous landscapes. One such study has been demonstrated in this letter, in which an upscaling algorithm based on averaging was implemented using RZSM estimates. The results presented in this letter have emphasized the importance of SM and LST simulations on multiple spatial scales under dynamic vegetation and heterogeneous land cover conditions for developing accurate SM retrieval and scaling algorithms.

Acknowledgment

The authors would like to thank the University of Florida High-Performance Computing Center for the computational resources and support, and for all of the model simulations conducted in this letter.

References

[1] Y. Kerr, P. Waldteufel, J. Wigneron, J. Martinuzzi, J. Font, and M. Berger, "Soil moisture retrieval from space: The Soil Moisture and Ocean Salinity (SMOS) mission," *IEEE Trans. Geosci. Remote Sens.*, vol. 39, no. 8, pp. 1729–1735, Aug. 2001.

[2] *Earth Science and Applications From Space: National Imperatives for the Next Decade and Beyond*, Nat. Res. Council, Washington, DC, 2007.

[3] B. Mohanty and T. Skaggs, "Spatio-temporal evolution and time stable characteristics of soil moisture within remote sensing footprints with varying soils, slopes, and vegetation," *Adv. Water Res.*, vol. 24, no. 9/10, pp. 1051–1067, 2001.

[4] I. Rodriguez-Iturbe, P. D'Odorico, A. Porporato, and L. Ridolfi, "On the spatial and temporal links between vegetation, climate, and soil moisture," *Water Res. Res.*, vol. 25, no. 12, pp. 3709–3722, 1999.

[5] C. Kim, J. Stricker, and R. Feddes, "Impact of soil heterogeneity on the water budget of the unsaturated zone," *Water Res. Res.*, vol. 33, no. 5, pp. 991–999, 1997.

[6] C. Kim and J. Stricker, "Influence of variable soil hydraulic properties and rainfall intensity on the water budget," *Water Res. Res.*, vol. 32, no. 6, pp. 1699–1712, Jun. 1996.

[7] C. Joshi and B. Mohanty, "Physical controls of near-surface soil moisture across varying spatial scales in an agricultural landscape during SMEX02," *Water Res. Res.*, vol. 46, pp. W12503-1–W12503-21, 2010.

[8] M. Cosh, T. Jackson, R. Bindlish, and J. Prueger, "Watershed scale temporal and spatial stability of soil moisture and its role in validating satellite estimates," *Remote Sens. Environ.*, vol. 92, no. 4, pp. 427–435, 2004.

[9] B. Mohanty, J. Famiglietti, and T. Skaggs, "Evolution of soil moisture spatial structure in a mixed-vegetation pixel during the SGP97 hydrology experiment," *Water Res. Res.*, vol. 36, no. 12, pp. 3675–3686, 2000.

[10] W. Crow and R. Reichle, "Land data assimilation activities in preparation of the NASA Soil Moisture Active Passive (SMAP) mission," in *Proc. WMO Data Assimil. Symp.*, Melbourne, Australia, 2009.

[11] W. Crow, S. T. K. Chan, D. Entekhabi, P. R. Houser, A. Y. Hsu, T. J. Jackson, E. G. Njoku, P. E. O'Neill, J. Shi, and X. Zhan, "An observing system simulation experiment for HYDROS radiometer-only soil moisture products," *IEEE Trans. Geosci. Remote Sens.*, vol. 43, no. 6, pp. 1289–1303, Jun. 2005.

[12] T. Bongiovanni, H. Enos, A. Monsivais-Huertero, B. Colvin, K. Nagarajan, J. Judge, P. Liu, J. Fernandez-Diaz, R. De Roo, Y. Goykhman, X. Duan, D. Preston, R. Shrestha, C. Slatton, M. Moghaddam, and A. England, Field observations during the Eighth Microwave, Water, and Energy Balance eXperiment (MicroWEX-8): From June 16 through August 24, 2009, Center Remote Sens., Univ. Florida, Gainesville, FL, Tech. Rep. [Online]. Available: http://edis.ifas.ufl.edu/ae476

[13] J. Casanova, F. Yan, M. Jang, J. Fernandez, J. Judge, C. Slatton, K. Calvin, T. Lin, O. Lanni, and L. W. Miller, Field observations during the Fifth Microwave, Water, and Energy Balance eXperiment (MicroWEX-5): From March 9 through May 26, 2006. Circular no. 1514, Center Remote Sens., Univ. Florida, Gainesville, FL, Tech. Rep. [Online]. Available: http://edis.ifas.ufl.edu/AE407

[14] T. Lin, J. Judge, K. Calvin, J. Casanova, M. Jang, O. Lanni, L. W. Miller, and F. Yan, Field observations during the Third Microwave, Water, and Energy Balance eXperiment (MicroWEX-3): From June 16 through December 21, 2004. Circular no. 1481, Center Remote Sens., Univ. Florida, Gainesville, FL, Tech. Rep. [Online]. Available: http://edis.ifas.ufl.edu/ae361

[15] Florida Automated Weather Network, 2011. [Online]. Available: http://fawn.ifas.ufl.edu/

[16] W. H. Brutsaert, "On a derivable formula for long-wave radiation from clear skies," *Water Res. Res.*, vol. 11, no. 5, pp. 742–744, 1975.

[17] J. Judge, A. England, J. Metcalfe, D. McNichol, and B. Goodison, "Calibration of an integrated land surface process and radio brightness (LSP/R) model during summertime," *Adv. Water Res.*, vol. 31, no. 1, pp. 189–202, 2008.

[18] J. Philip and D. de Vries, "Moisture movement in porous materials under temperature gradients," *Trans. Amer. Geophys. Union*, vol. 38, no. 2, pp. 222–232, 1957.

[19] D. de Vries, "Simultaneous transfer of heat and moisture in porous media," *Trans. Amer. Geophys. Union*, vol. 39, no. 5, pp. 909–916, 1958.

[20] J. Judge, A. England, C. Crosson, B. Hornbuckle, D. Boprie, E. Kim, and Y. Lieu, "A growing season land surface process/radio brightness model for wheat-stubble in the Southern Great Plains," *IEEE Trans. Geosci. Remote Sens.*, vol. 37, no. 5, pp. 2152–2158, Sep. 1999.

[21] J. Judge, A. England, J. Metcalfe, D. McNichol, and B. Goodison, "Calibration of an integrated land surface process and radio brightness (LSP/R) model during summertime," *Adv. Water Res.*, vol. 31, no. 1, pp. 189–202, 2008.

[22] B. Whitfield, J. Jacobs, and J. Judge, "Intercomparison study of the land surface process model and the common land model for a prairie wetland in Florida," *J. Hydrometeorol.*, vol. 7, no. 6, pp. 1247–1258, 2006.

[23] Y. Chung, "A snow-soil-vegetation-atmosphere-transfer/radio brightness model for wet snow," Ph.D. dissertation, Univ. Michigan, Ann Arbor, MI, 2007.

[24] J. Casanova and J. Judge, "Estimation of energy and moisture fluxes for dynamic vegetation using coupled SVAT and crop-growth models," *Water Res. Res.*, vol. 44, pp. W07415-1–W07415-20, 2008.

[25] S. Verseghy, N. McFarlane, and M. Lazare, "CLASS—A Canadian land surface scheme for GCMs, II vegetation model and coupled runs," *Int. J. Climatol.*, vol. 13, no. 4, pp. 347–370, May/Jun. 1993.

[26] K. Trenberth, *Climate System Modeling*. New York: Cambridge Univ. Press, 1995.

[27] J. Peixoto and A. Oort, *Physics of Climate*. New York: AIP, 1992.

[28] J. Jones, G. Hoogenboom, C. Poter, K. Boote, W. Hunt, P. Wilkens, U. Singh, A. Gijsman, and J. Ritchie, "The DSSAT cropping system model," *Eur. J. Agron.*, vol. 18, no. 3/4, pp. 235–265, Jan. 2003.

[29] K. Boote and J. Jones, *Simulation of Crop Growth*. New York: Marcel Dekker, 1998.

[30] T. Mavromatis, K. Boote, W. James, G. Wilkerson, and G. Hoogenboom, "Repeatability of model genetic coefficients derived from soybean performance trials across different states," *Crop Sci.*, vol. 42, no. 1, pp. 76–89, Jan. 2002.

[31] J. Casanova, J. Judge, and J. Jones, "Calibration of the ceres-maize model for linkage with a microwave remote sensing model," *Trans. Amer. Soc. Agricult. Biol. Eng.*, vol. 49, no. 3, pp. 783–792, 2006.